NASA
Technical
Paper
2280

AVSCOM
Technical
Report
83-C-6

February 1984

Preliminary Study of Thermomechanical Fatigue of Polycrystalline MAR-M 200

Robert C. Bill,
Michael J. Verrilli,
Michael A. McGaw,
and Gary R. Halford

NASA

NASA Technical Paper 2280

AVSCOM Technical Report 83-C-6

1984

Preliminary Study of Thermomechanical Fatigue of Polycrystalline MAR-M 200

Robert C. Bill
Propulsion Laboratory
USAAVSCOM Research and Technology Laboratories
Lewis Research Center
Cleveland, Ohio

Michael J. Verrilli
Northwestern University
Evanston, Illinois

Michael A. McGaw
and Gary R. Halford
Lewis Research Center
Cleveland, Ohio

National Aeronautics
and Space Administration

Scientific and Technical Information Branch

Summary

Currently used life prediction methods were developed to handle isothermal fatigue and creep-fatigue problems. Actual gas turbine components, however, are subjected to both mechanical strains and temperatures that vary cyclically with time. In this work, polycrystalline MAR-M 200 specimens were exposed to both in-phase (maximum tensile strain simultaneous with maximum temperature) and out-of-phase (maximum compressive strain simultaneous with maximum temperature) thermomechanical fatigue (TMF) cycling.

Thermomechanical fatigue experiments were conducted over a cyclic temperature range of 500° to 1000° C. Inelastic strain ranges of 0.03 to 0.2 percent were imposed on the specimens. TMF lives were found to be significantly shorter than isothermal low-cycle-fatigue (LCF) life at the maximum cycle temperature, and in-phase cycling was more damaging than out-of-phase cycling. Extensive crack tip oxidation appeared to play a role in promoting the severity of in-phase cycling. Carbide particle-matrix interface cracking was also observed after in-phase cycling. The applicability of various life prediction models to the TMF results obtained was assessed. The models considered included strainrange partitioning, spanning factor, Ostergren's model, frequency separation, and an oxidation model. It was concluded that current life prediction models based on isothermal data as input must be modified to be applicable to the TMF results.

Introduction

Currently used methods of life prediction and material constitutive modeling for high-temperature gas turbine components usually are based on isothermal data. In reality these components are subjected to both temperatures and mechanical strains that vary with time. Throughout cyclic exposure the microstructure of the material may never reach an equilibrium state. Also, there are no extensive experimental bases for estimating nonisothermal cyclic damage accumulation and material constitutive behavior. Indeed, the integrated effects of damage accumulated over a temperature range are virtually unexplored.

Conditions under which a material specimen is subjected to both temperatures and mechanical strains that vary cyclically constitute what is known as thermomechanical fatigue (TMF). Thermal fatigue experimental evaluations (refs. 1 and 2) incorporate some of the effects present in thermomechanical fatigue but suffer from the drawback that the thermal cycle and the mechanical cycle are inevitably coupled in such a manner that cycle parameters cannot be controlled with any degree of independence.

Developing life prediction capabilities that are directly applicable to nonisothermal situations requires a data base in which temperature and mechanical strain are both independently controlled as a function of time. On this basis it is possible, in principle, either to adapt existing isothermal life prediction methods to TMF or to develop new life prediction methods.

Review of the TMF Literature

Some TMF studies performed on various materials are cited in order to illustrate general experimental trends and approaches to adapting isothermal life prediction concepts to TMF conditions. Though not an exhaustive literature survey, the cited work provides a perspective from which to view the present work.

Taira et al. (ref. 3) conducted TMF experiments on 1016 carbon steel and AISI 347 stainless steel and compared their results with isothermal data. They found good correlation between TMF lives and isothermal lives determined at the maximum and minimum temperatures associated with the TMF cycle by invoking a "spanning factor" for use in conjunction with a linear damage accumulation rule. In effect, the spanning factor is a proportionality constant based on isothermal lives at the TMF temperature extremes. The approach is not likely to be generally valid when there is strong interaction among the damage mechanisms operating over the temperature range of the TMF cycle.

Lundberg and Sandstrom (ref. 4) have shown that strainrange partitioning (SRP) concepts might be used for qualitative extrapolation of isothermal life prediction to TMF situations. In particular, thermal fatigue results for Cr-Mo and 18Cr-10Ni steels could be rationalized on the basis of isothermal SRP data. Lundberg and Sandstrom offer a generally applicable cautionary note, however. Their observations and those of Taira are not applicable to cycle conditions (temperature ranges and hold times) over which microstructural changes to the alloy might be expected.

Halford and Manson (ref. 5) have successfully applied SRP to TMF life prediction for AISI 316 stainless steel. They point out that AISI 316 stainless steel is a material whose basic cyclic strain-life relations are not temperature dependent. Special procedures that have yet to be developed are needed to cope with temperature-dependent materials.

Rau, Gemma, and Leverant (ref. 6) investigated crack propagation under in-phase (maximum tensile strain simultaneous with maximum temperature) and out-of-phase (maximum compressive strain simultaneous with maximum temperature) TMF cycling, as well as under isothermal cycling conditions for some nickel-based superalloys. Crack propagation rates were observed to be much higher for out-of-phase cycling than for in-phase cycling. Also, crack propagation rates under TMF

conditions were higher than under comparable (mechanistically) isothermal cycling conditions. A compressive-creep-assisted crack sharpening mechanism was proposed, but not verified, to account for rapid out-of-phase crack propagation.

Objective and Scope

In this work, TMF results obtained from polycrystalline MAR-M 200 are summarized and compared with isothermal LCF results. Both in-phase and out-of-phase TMF cycling were investigated, and the temperature range employed was 500° to 1000° C. Inelastic strain ranges of 0.03 to 0.2 percent were investigated. All experiments were conducted in room-temperature air.

This investigation was conducted to determine the effect of TMF cycle type on cyclic life and to compare TMF life with isothermal LCF life for polycrystalline MAR-M 200. The basic life data were supplemented by cyclic stress-strain hysteresis loop measurements and by metallographic and fractographic observations of crack initiation and propagation mechanisms.

Materials

The certified composition of the MAR-M 200 alloy used in this investigation is summarized in table I. This alloy was conventionally cast into thin-wall tubes (1.5 mm thick) with an equiaxed grain size of approximately 75 μm. These tubes were machined into hollow cylindrical specimens conforming to the geometry and dimensions shown in figure 1. Experiments were conducted with these specimens in the as-cast condition, for which the hardness was Rockwell C-38.

Apparatus and Procedure

Test specimens were heated by using a direct resistance technique, and strain was measured by means of a diametral extensometer system as described in reference 7. Both the thermal cycle and the mechanical strain cycle were controlled through use of arbitrary waveform generators.

All tests were performed on a servocontrolled testing system under diametral strain control. The cyclic frequency employed in TMF testing was 3.7×10^{-3} Hz. Isothermal tests that did not include a hold time (PP tests, i.e., no creep) were conducted at a 0.5-Hz cyclic frequency. Isothermal test at 927° C that did include both a tensile and compressive hold time (CC tests) were conducted at frequencies from 5.7×10^{-5} to 2.1×10^{-2} Hz. The waveform for all cyclic tests was sinusoidal.

Temperature was also servocontrolled by using control thermocouples mounted on the specimen for the feedback signal. The control thermocouples were as close as possible to the minimum section of the specimen without introducing crack initiation sites during the spot welding. A special calibration specimen was employed to compare the output of a thermocouple located at the center of the gage section (minimum section) with that of a control thermocouple located 3 mm away from the minimum section. The calibration experiments showed that the maximum temperature difference between a control

TABLE I. – COMPOSITION OF POLYCRYSTALLINE MAR-M 200

Ni	Co	Cr	Al	Ti	W	C	Fe	S	Si	Cb	Zr	B	Cu	Mn
Bal.	10.3	9.2	5.21	2.13	12.55	0.12	0.63	0.003	0.073	0.96	0.043	0.015	<0.1	<0.02

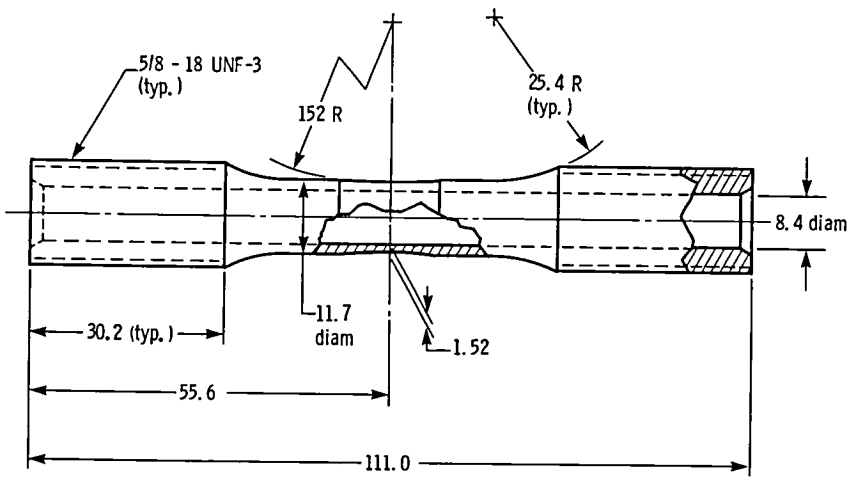

Figure 1. – Specimen configuration. (Dimensions are in mm, except screw thread designation.)

thermocouple and the calibration thermocouple was 10° C at the maximum cycle temperature.

Once a specimen had been assembled into the load frame with the diametral strain measurement device and control thermocouples attached and the load was zeroed, the specimen was strained elastically at several selected temperatures within the temperature limits of the thermomechanical test. At each selected temperature the load versus displacement was recorded. The slope of the lines obtained was E/μ_e, where E is the elastic modulus and μ_e is the elastic Poisson's ratio. This was plotted versus temperature and used in the data reduction.

With the servocontroller in load control, the sample was allowed to thermally cycle under zero load while fine adjustments of the upper temperature were made. After a few cycles the specimen and extensometer system reached a dynamic thermal equilibrium and a plot of temperature versus thermal strain was recorded.

The calculated span setting that exactly offsets the total thermal strain values on the plot defines the "zero" point. Now, with cyclic operation under the control of the wave generator, any span setting above the zero point will result in the maximum temperature occurring at the maximum compressive strain (this is designated as "an out-of-phase test"). Any span setting below the zero point will result in the maximum temperature occurring at the maximum tensile strain (in-phase test). Both in-phase and out-of-phase cycles are illustrated schematically in figure 2.

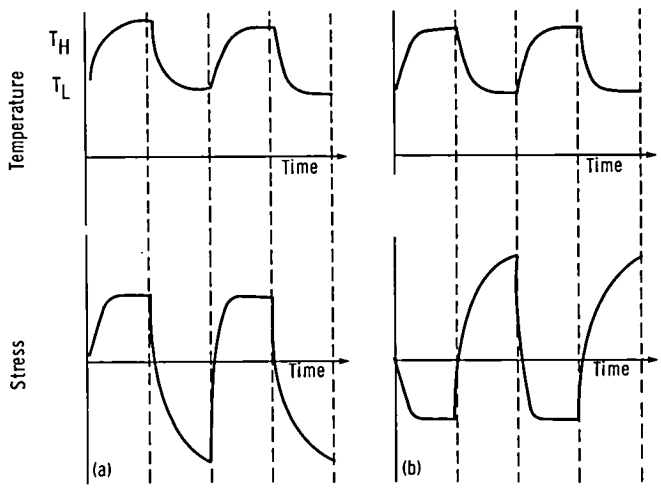

(a) In phase. (b) Out of phase.

Figure 2. – Schematics of in-phase and out-of-phase thermomechanical fatigue cycles.

Results

TMF Experiments

Reduction of the diametral strain measurements involves subtracting the free thermal expansion contribution from the stabilized load-displacement loop and replotting the loop as a rectified stress-versus-mechanical-strain hysteresis loop. The relation between total longitudinal mechanical strain ϵ_T^L and total diametral mechanical strain $\epsilon_{T,M}^D$ is given by

$$\epsilon_T^L = 2\left(\epsilon_{T,M}^D - \frac{\sigma\mu_e}{E}\right) + \frac{\sigma}{E} \qquad (1)$$

The total diametral mechanical strain is related to the diametral measurements through

$$\epsilon_{T,M}^D = \epsilon_T^D - \epsilon_{FE} \qquad (2)$$

Here, ϵ_T^D is the total measured diametral strain and ϵ_{FE} is the free thermal expansion contribution determined from the temperature-versus-diametral-strain curve at zero stress.

A typical stabilized stress-versus-diametral-total-strain loop is shown in figure 3 along with a temperature-versus-diametral-free-expansion plot. Application of equation (1), point by point around the loop, resulted in the axial stress–mechanical strain hysteresis loop shown in figure 4. Such loops were constructed for each TMF experiment, and the important cycle parameters are summarized in table II.

The inelastic axial strain range is plotted versus the number of cycles to failure in figure 5. Results are shown for in-phase and out-of-phase TMF experiments as well as isothermal fatigue data at 1000°, 927°, and 650° C. Table III summarizes the isothermal data in terms of SRP. A few observations are immediately noteworthy. First, there was a marked sensitivity of TMF life to the type of cycle imposed. The life of polycrystalline MAR-M 200 was considerably shorter under in-phase cycling conditions than under out-of-phase cycling condi-

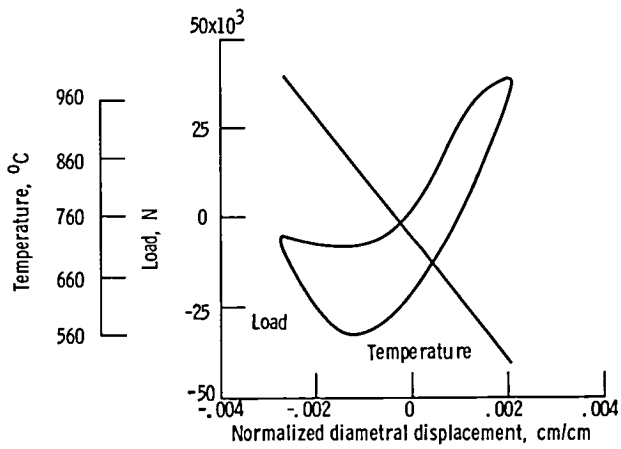

Figure 3. – Stabilized load-displacement loop and temperature displacement plot for out-of-phase specimen HH-52.

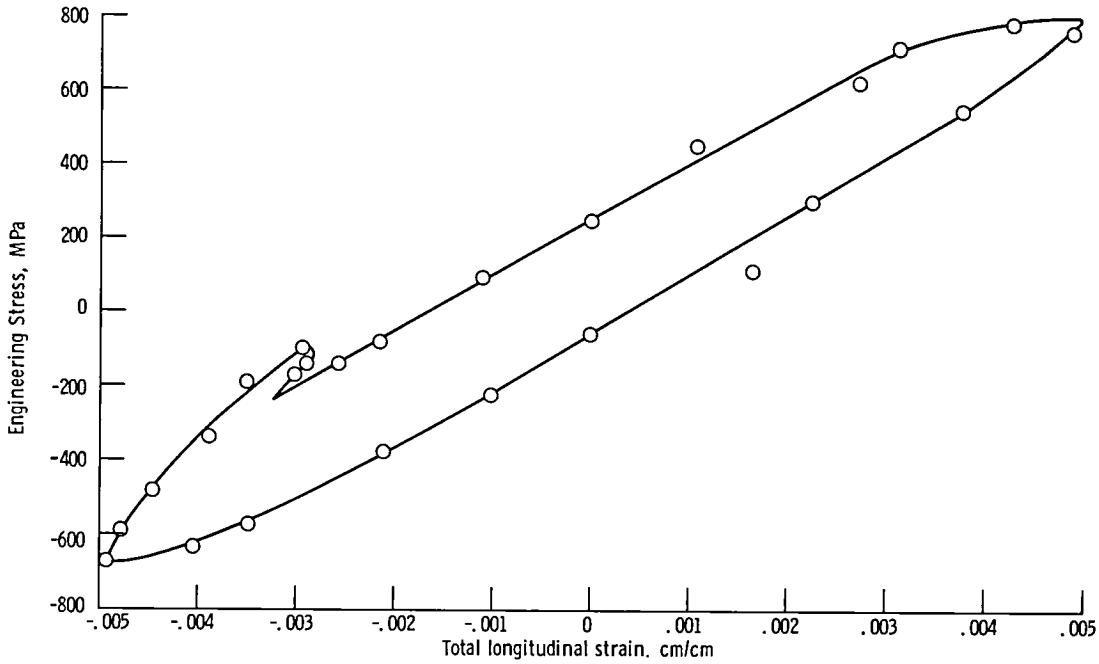

Figure 4. – Rectified hysteresis loop for out-of-phase specimen HH-52, cycle 43.

TABLE II. – TMF CYCLE PARAMETERS FOR POLYCRYSTALLINE MAR-M 200

[All tests were run at a frequency of 0.00366 Hz (4.55 min/cycle).]

Specimen	Tensile stress, MPa	Compressive stress, MPa	Total stress range, MPa	Elastic strange range, cm/cm	Inelastic strain range, cm/cm	Total strain range, cm/cm	Number of cycles to failure, N_f	Temperature range, °C	In or out of phase ?
HH-53	616	493	802	0.00369	0.00059	0.00428	1304	492 – 1000	Out of phase
HH-58	808	627	1440	.00817	.00137	.00954	233	494 – 1002	Out of phase
HH-52	825	703	1520	.00825	.00202	.00946	60	496 – 1001	Out of phase
HH-57	360	925	1290	.00755	.00219	.00974	25	492 – 1001	In phase
HH-17	209	813	1020	.00593	.00038	.00631	161	496 – 1000	In phase
HH-61	208	843	1050	.00625	.00083	.00708	117	495 – 1002	In phase
HH-66	213	800	1020	.00740	.00058	.00798	73	499 – 1002	In phase

tions. The significance of the apparent difference in slope between the in-phase and out-of-phase life lines is uncertain; additional data are required to substantiate this difference. Second, TMF lives, especially under in-phase cycling conditions, were considerably shorter than isothermal lives at 1000° and 927° C. Third, for a given inelastic strain range, the isothermal life showed a notable sensitivity to temperature. However, the isothermal LCF life of MAR-M 200 appeared to be relatively insensitive to the type of isothermal cycle imposed. The inclusion of tensile and compressive hold times did not result in significant changes in cyclic fatigue life. At 927° C for example, a CC test lasting over 1000 hr had a cyclic lifetime no different from PP tests lasting only 0.2 hr. The TMF tests had exposure times at high temperatures that were greater than those for the isothermal PP tests but less than those for the isothermal CC tests. Thus, time at temperature by itself does not appear to be a critical factor from the standpoint of governing cyclic life.

Metallography and Fractography

A fractographic study conducted on a specimen subjected to in-phase cycling (number of cycles to failure $N_f = 25$) is summarized in figure 6. In this particular case the dominant crack began at the spherical inclusion particle adjacent to the outer surface. Observe also that the fracture surface exhibits the faceted topography generally associated with intergranular propagation. Metallographic sections from the same specimen or a similar specimen ($N_f = 117$), shown in figure 7, indicate that crack propagation is in fact intergranular under in-

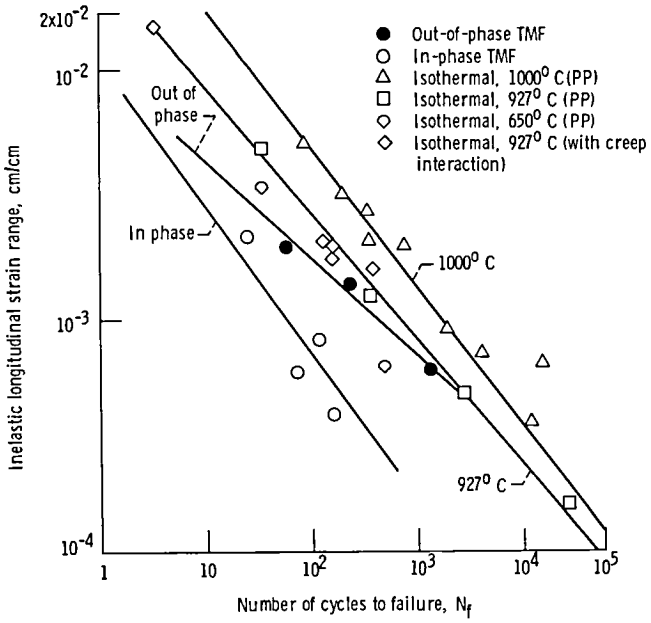

Figure 5. – Inelastic strain range as function of number of cycles to failure for polycrystalline MAR-M 200 under thermomechanical fatigue and isothermal cycling conditions.

phase cycling and that there are numerous internal crack initiation sites at grain boundaries.

Metallographic sections were also made through the fracture surface of specimens subjected to out-of-phase cycling, a typical example of which is shown in figure 8 (N_f= 1304). There is evidence of mixed transgranular and intergranular crack growth, with about one-third of the fracture surface being clearly transgranular.

Close inspection of metallographic sections in regions somewhat away from the primary fracture surface, but containing surface-connected cracks, reveals a consistent difference between in-phase and out-of-phase specimens. Figure 9(a) (in phase) shows evidence of extensive oxidation of the crack surface and the secondary crack tips (N_f= 117). The out-of-phase cycled specimen (fig. 9(b)) shows considerably less oxidation of the crack surface and virtually no accumulation of oxidized material at the crack tips (N_f= 233).

The interaction of carbides with the propagating cracks appeared to be different for in-phase and out-of-phase cycling. For in-phase cycling, as shown in figures 10(a) and (b), considerable oxidation of the $\gamma-\gamma'$ matrix occurred around the interface with a carbide particle directly in front of a crack. Also, the matrix pulled away from the particle interface, probably assisted by grain boundary oxidation ahead of the crack. In contrast, out-of-phase cycling, shown in figures 10(c) and (d), resulted in fracture of the carbides but with the retention of sound carbide-matrix interfaces.

The morphology of the $\gamma-\gamma'$ matrix changed considerably after exposure to out-of-phase cycling but retained its original blocky γ' particulate structure after in-phase cycling, as is summarized in figure 11. Figures 11(a) and (b) (in-phase cycling) show the continuous γ,

TABLE III. – SUMMARY OF ISOTHERMAL DATA

Specimen	Cycle type[a]	Frequency, Hz	Temperature, °C	Total stress range, MPa	Elastic strain range, cm/cm	Inelastic strain range, cm/cm	Number of cycles to failure, N_f	Time to failure, min
HH-41	PP	0.5	1000	601	0.0043	0.0020	760	25
HH-43				745	.0053	.0054	88	3
HH-69				385	.0028	.0007	15 390	513
HH-54				425	.0030	.0007	4 057	138
HH-18				730	.0053	.0033	195	7
HH-44				629	.0046	.0021	335	11
HH-48				625	.0046	.0028	338	11
HH-49				501	.0038	.0009	1 961	65
HH-33				369	.0027	.0004	11 817	394
HH-2			927	1710	.0096	.0052	35	1.2
HH-73				680	.0043	.0046	2 735	91
HH-40		.8		586	.0037	.0002	26 020	543
HH-38		1.0		975	.0062	.0012	357	6
HH-35	CP	5.0×10^{-3}		760	.0048	.0019	160	533
HH-37	CP	0.76×10^{-3}		632	.0040	.0016	380	8300
HH-28	PC	21×10^{-3}		850	.0052	.0018	160	127
HH-21	CC	0.057×10^{-3}		765	.0049	.0170	3.5	1002
HH-22	CC	1.1×10^{-3}		540	.0034	.0021	130	1970
HH-74	PP	0.5	648	1630	.0120	.0027	482	16
HH-3	PP	1×10^{-2}	648	1780	.0098	.0036	36	60

[a]PP denotes isothermal tests that did not include a hold time (i.e., no creep); CC denotes isothermal tests that included both a tensile and compressive hold time; CP denotes isothermal tests that include a tensile hold time; PC denotes isothermal tests that include a compressive hold time.

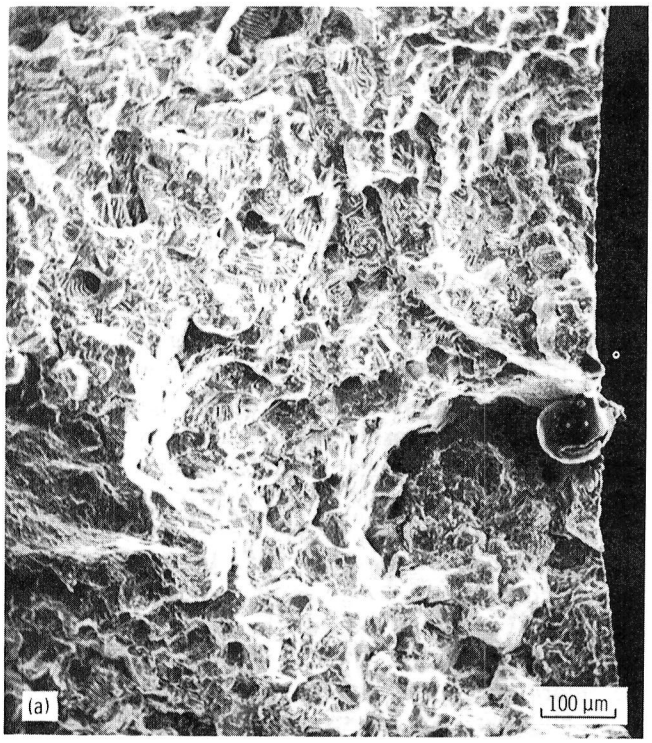

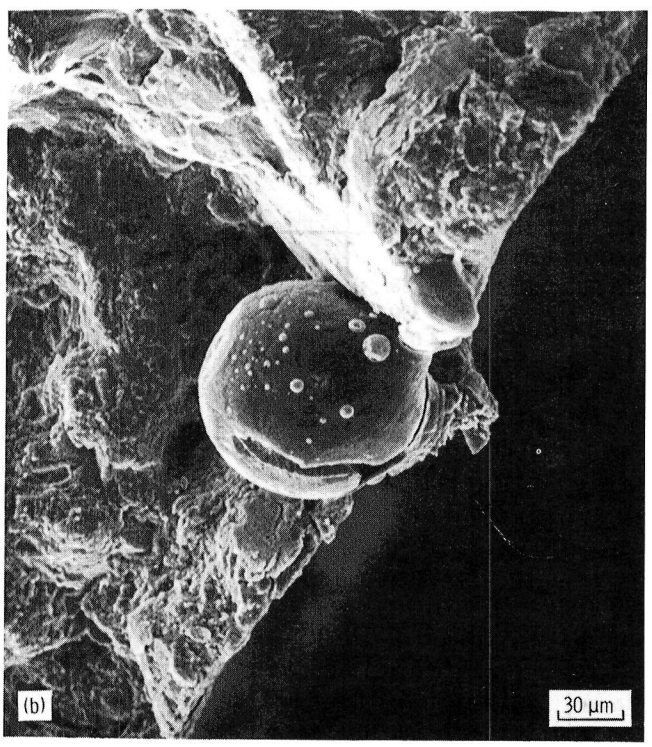

(a) Overview of fracture surface.
(b) Possible initiation site.

Figure 6. – SEM fractographs of MAR-M 200 after in-phase cycling to failure (specimen HH-57, $N_f = 25$).

blocky γ' particulate microstructure throughout most of the matrix with some distortion of the γ' particles near the grain boundary cracks and carbide particles. In contrast, after exposure to out-of-phase cycling (figs. 11(c) and (d)), the γ' particles have deformed to the extent that the original blocky structure is no longer apparent. In fact, the γ' phase shows a considerable degree of two-dimensional continuity in figures 11(c) and (d). The inelastic strain ranges were nearly identical for the in-phase and out-of-phase tests, and since the out-of-phase specimen had nearly 20 times the life, it also underwent 20 times the amount of cyclic deformation.

Discussion

Life Prediction

In this section, the applicability of several isothermal life prediction models to the present TMF results is considered. Also, the spanning factor concept proposed by Taira et al. (ref. 3) is given consideration. The isothermal life prediction models that are assessed include SRP (ref. 8), the Ostergren model (ref. 9), the Coffin frequency separation model (ref. 10), and Antolovich's oxidation model (ref. 11).

Consider first the application of the spanning factor concept to the results obtained for polycrystalline MAR-M 200. Following literally the approach outlined by Taira et al. (ref. 3), the calculated TMF life turned out to be about 1000 cycles for a 0.1-percent inelastic strain range. The actual TMF life for in-phase cycling was only 58 cycles, and that for out-of-phase cycling was only 425 cycles. The calculation, summarized in the appendix, is based on extrapolation of isothermal LCF life data for 0.1-percent strain range down to 500° C. If one redefines some of the terms used by Taira et al. so that N_f (T_1) is the longer isothermal life corresponding to one of the TMF cycle temperature limits and N_f (T_2) is the shorter life, the predicted TMF life turns out to be about 62 cycles. Although this calculation is in better agreement with the in-phase experimental results, it is in very poor agreement with the out-of-phase experimental results. The difficulties with the spanning factor approach are now clearly apparent. First, the present formulation of the spanning factor does not account for cycle phasing effects, which were found to be very strong for polycrystalline MAR-M 200. Second, it is not clear a priori how to define the isothermal life terms. It would seem that Taira et al. made the tacit assumption that isothermal lives should be shorter at high temperatures than at low temperatures—an assumption that may be true for certain alloys, but not so for polycrystalline MAR-M 200 and many other materials (ref. 12) that become more ductile as temperature is increased. Numerous nickle-based alloys follow this trend.

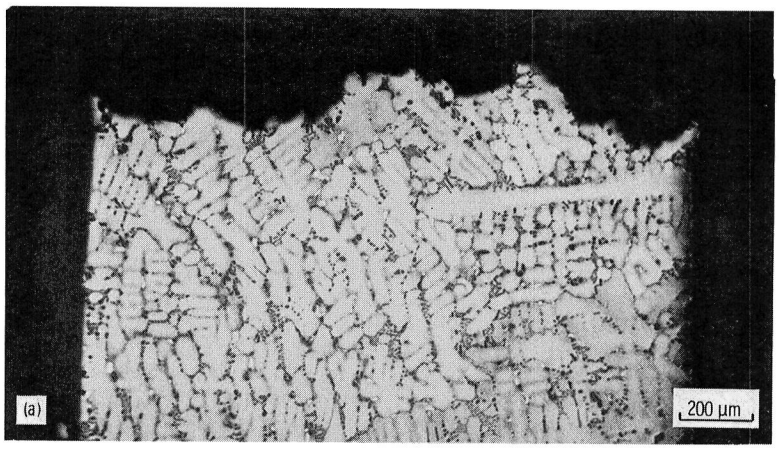

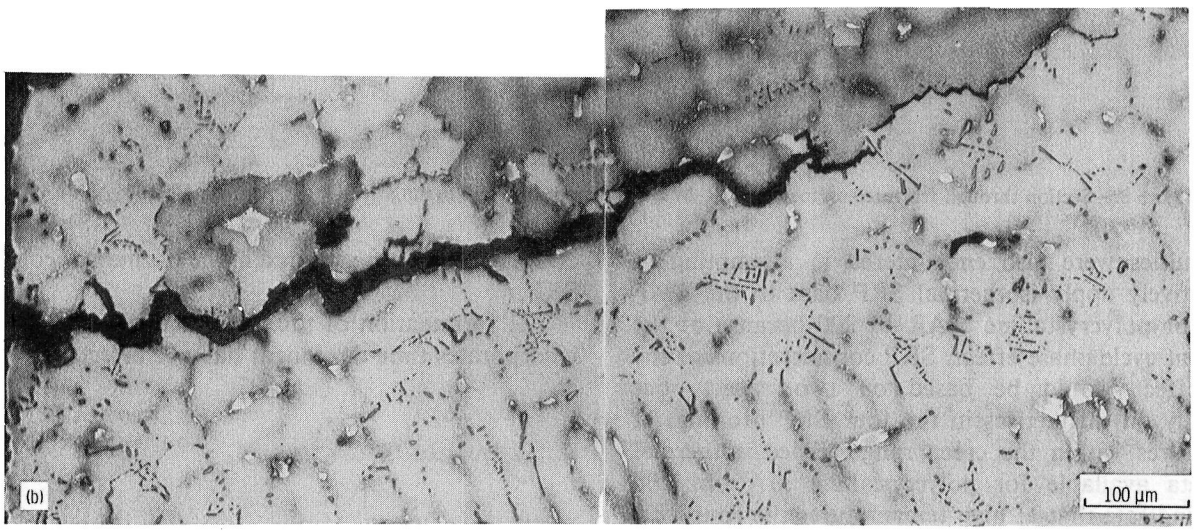

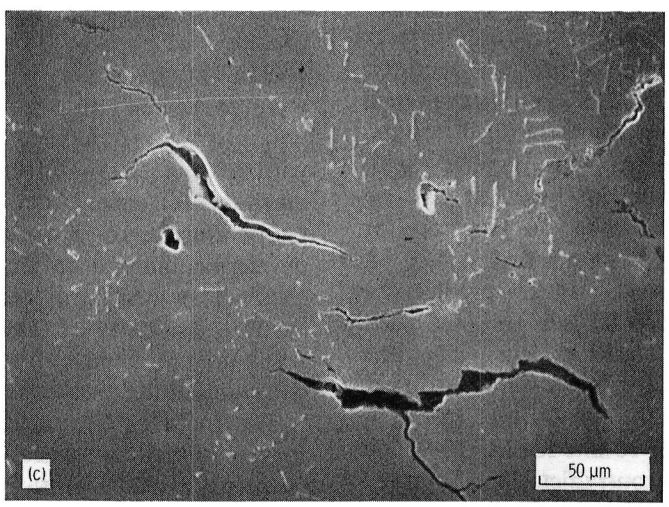

(a) Section through fracture surface (specimen HH-57, $N_f = 25$).
(b) Surface-initiated intergranular crack (specimen HH-61, $N_f = 117$).
(c) Internal grain boundary cracks (specimen HH-61, $N_f = 117$).

Figure 7. – Metallographic sections from MAR-M 200 after in-phase cycling to failure.

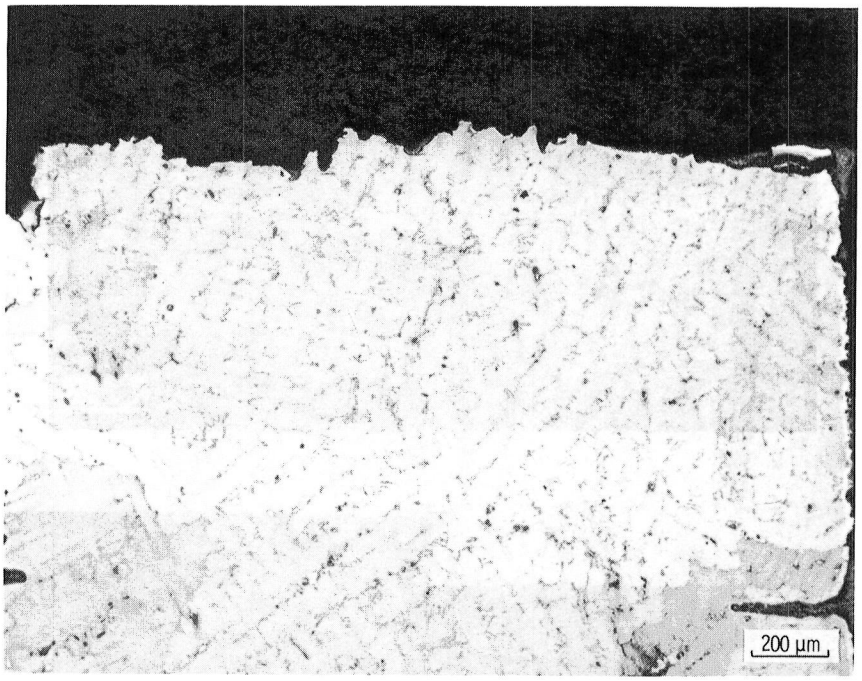

Figure 8. – Section through fracture surface of MAR-M 200 after out-of-phase cycling to failure (specimen HH-53, $N_f = 1304$).

Difficulties were also encountered in attempting to quantitatively apply isothermal SRP data to the TMF results for polycrystalline MAR-M 200 because of the significant cycle phase effect. SRP considerations of the phase effect would be based on two aspects but principally on differences in the four SRP life lines at temperatures within the creep range. Since isothermal SRP data available for polycrystalline MAR-M 200 (ref. 8) indicate that at high temperatures the four SRP life lines are quite close together, the observed TMF effect would not be expected. Thus, the other aspect, based on the variation of SRP life relations with temperature (determined either through direct experiment or through estimation using the ductility-normalized SRP relations of ref. 13) should be examined to see if the variation is consistent with the TMF results. Although a vigorous procedure for dealing with continuous temperature variation has yet to be developed, a life calculation based on extreme, or boundary, conditions could be applied. Such a calculation was used in reference 14 to predict the thermal fatigue life of a René 80 gas turbine blade subjected to factory engine testing. René 80, like MAR-M 200, exhibits lower fatigue resistance at lower test temperatures. Applying the procedures used in reference 14 to the present TMF results for MAR-M 200 resulted in life predictions that contradicted the observed phase effects. Specifically, out-of-phase TMF lives were calculated to be less than in-phase TMF lives, a prediction that is opposite the observed experimental results. Apparently the TMF experiments are introducing effects that are not captured in the isothermal concepts of SRP.

The formulation of the Ostergren model (ref. 9) that incorporates time-dependent damage effects is expressed as

$$\sigma_T \, \Delta\epsilon_p [N_f \nu^{(k-1)}]^{\beta} = C$$

where σ_T is the peak tensile stress; $\Delta\epsilon_p$, the inelastic strain range; N_f, the number of cycles to failure; ν, the cyclic frequency; and k, $\beta(<0)$, and C, temperature-dependent constants. It appears that the Ostergren model would predict in-phase lives to be higher than out-of-phase lives because of the way σ_T is incorporated. If the frequency were partitioned into compression-going and tension-going terms and these terms were somehow normalized with respect to an intrinsic material (microstructural, mechanistic) relaxation time over the TMF cycle temperature span, a working model for TMF might be developed. Such a development effort would require a clear understanding of controlling damage mechanisms, the rate sensitivity of these mechanisms to temperature, and a prudent choice of isothermal life data to define the constants in the present Ostergren model.

The frequency separation model (10) written in the form that includes tension-going and compression-going frequency terms is given by

$$N_f = D \, \Delta\epsilon_p^a \nu_t^b \left(\frac{\nu_c}{\nu_t}\right)^c$$

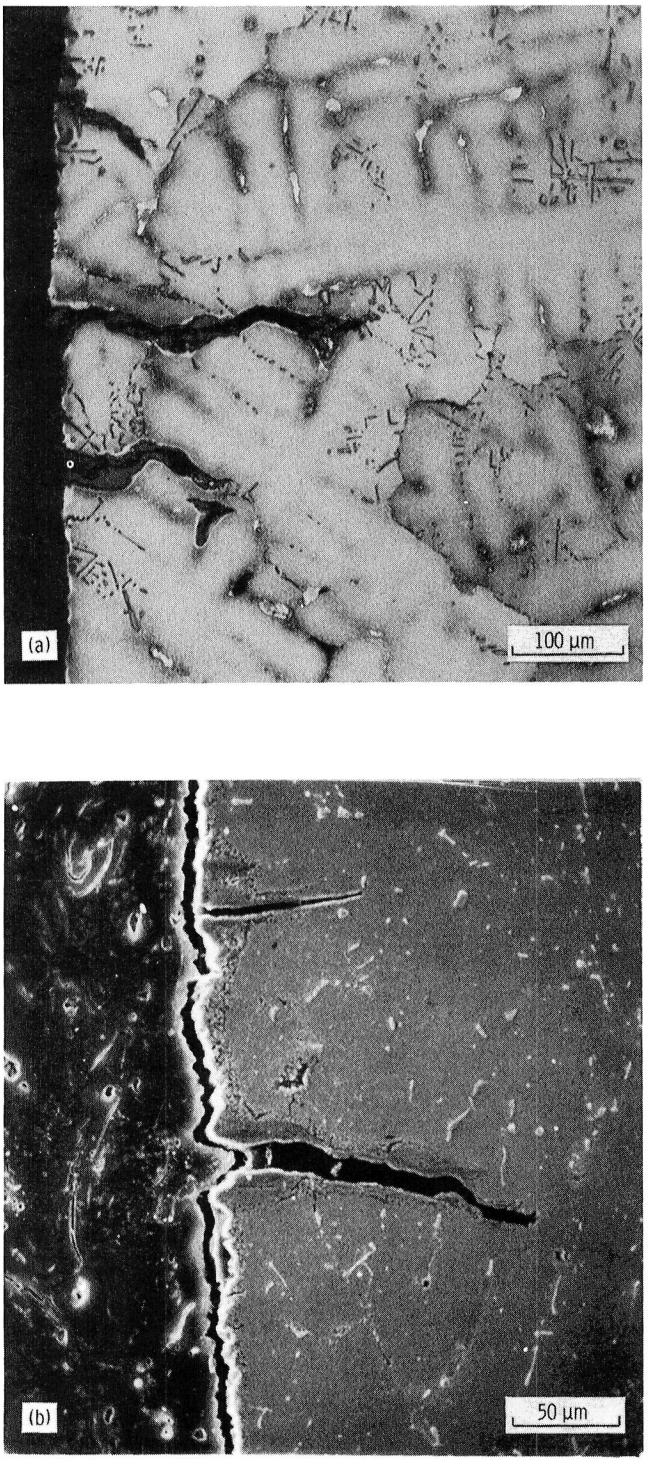

(a) In-phase (specimen HH-61, $N_f = 117$).
(b) Out-of-phase (specimen HH-58, $N_f = 233$).

Figure 9. – Oxidation of crack surfaces on MAR-M 200 after in-phase and out-of-phase thermomechanical fatigue cycling.

where ν_t and ν_c are tension- and compression-going frequencies, respectively, and a, b, c, and D are temperature-dependent constants. As with the Ostergren model, normalization of the frequency terms with respect to material response and judicious choice of isothermal life data-base conditions might provide a sound basis for developing a TMF life prediction model.

Antolovich's oxidation model (ref. 11) describes surface initiation of microcracks within a growing oxide film. As presently formulated, no feature addressing in-phase or out-of-phase TMF phenomena is included. If the model were to incorporate the reasonable supposition that crack initiation occurs within the film under the low-temperature tensile portion of the TMF cycle after film growth under high-temperature compression, one would expect out-of-phase cycling to be more damaging than in-phase cycling. This behavior is inconsistent with the present results. Perhaps the oxidation model can be reformulated to describe cyclic-oxidation-assisted crack growth due to rapid oxidation of the crack tip material.

Metallurgical Considerations

Besides the effect on TMF life, the TMF cycle phasing was observed to have a notable effect on microstructure and damage mechanisms. However, the fact that all metallurgical and metallographic studies were done on failed specimens must be kept in mind in interpreting apparent mechanistic and microstructural dependence on TMF phasing. In particular, the distortion of the γ' structure observed after out-of-phase cycling may have been due to the significantly higher (20 times) number of cycles to failure and higher accumulated strains for out-of-phase cycling than for in-phase cycling. On the other hand, the crack tip oxidation effects and possibly the carbide particle interaction effects noted for in-phase cycling appear all the more damaging when it is considered that total test time, number of cycles, and cumulative strains are much smaller for in-phase cycling than for out-of-phase cycling. Very likely, the tendency for cracks to open at high temperature under in-phase cycle conditions promoted rapid oxidation of crack tips and crack surfaces and internal oxidation of matrix, grain boundary, and carbide-matrix interfaces near crack tips.

TMF life prediction methods should account for the different deformation and damage mechanisms that can occur over the temperature range of the TMF cycle. For example, at the high-temperature portion of the TMF cycle employed in this study, cube slip systems can become activated (ref. 15) and unpaired dislocation slip can occur in the γ' particles (ref. 16). Deformation by mechanical microtwinning initiated in the γ' particle is observed at temperatures above 600° C in some $\gamma - \gamma'$ alloy systems (ref. 17). Also, a generally more homogeneous dislocation distribution is seen above 800° C, resulting from the increased ease of thermally assisted climb and cross slip (ref. 17). At the low-temperature portion, however, γ' particles must deform by planar shearing on an octahedral system through a paired

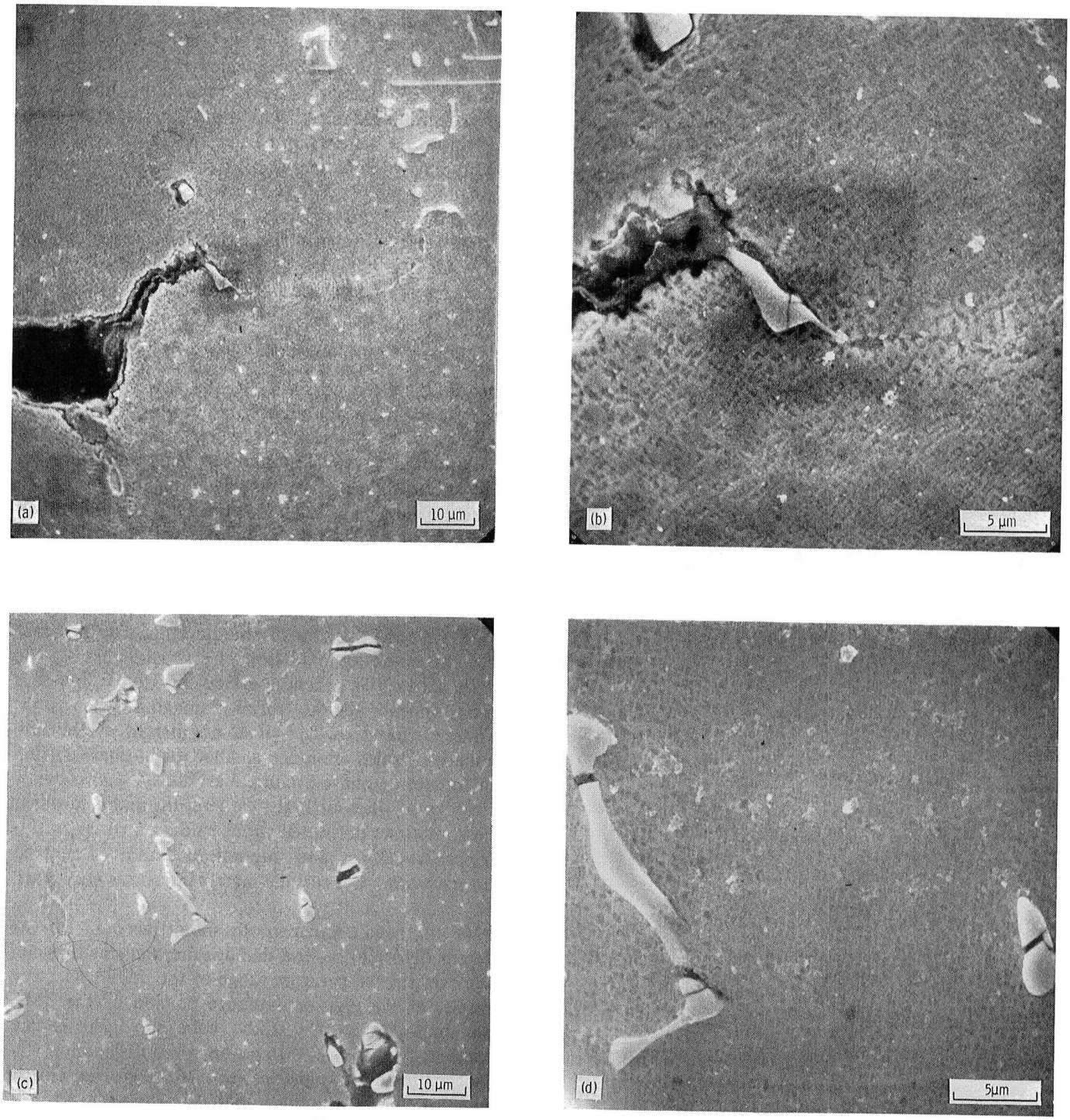

(a) In phase, overview of crack tip (specimen HH-57, $N_f = 25$).
(b) In phase, carbide particle detail (specimen HH-57, $N_f = 25$).
(c) Out of phase, typical section (specimen HH-52, $N_f = 60$).
(d) Out of phase, carbide particle detail (specimen HH-52, $N_f = 60$).

Figure 10. – Role of carbides in MAR-M 200 after in-phase and out-of-phase thermomechanical fatigue cycling.

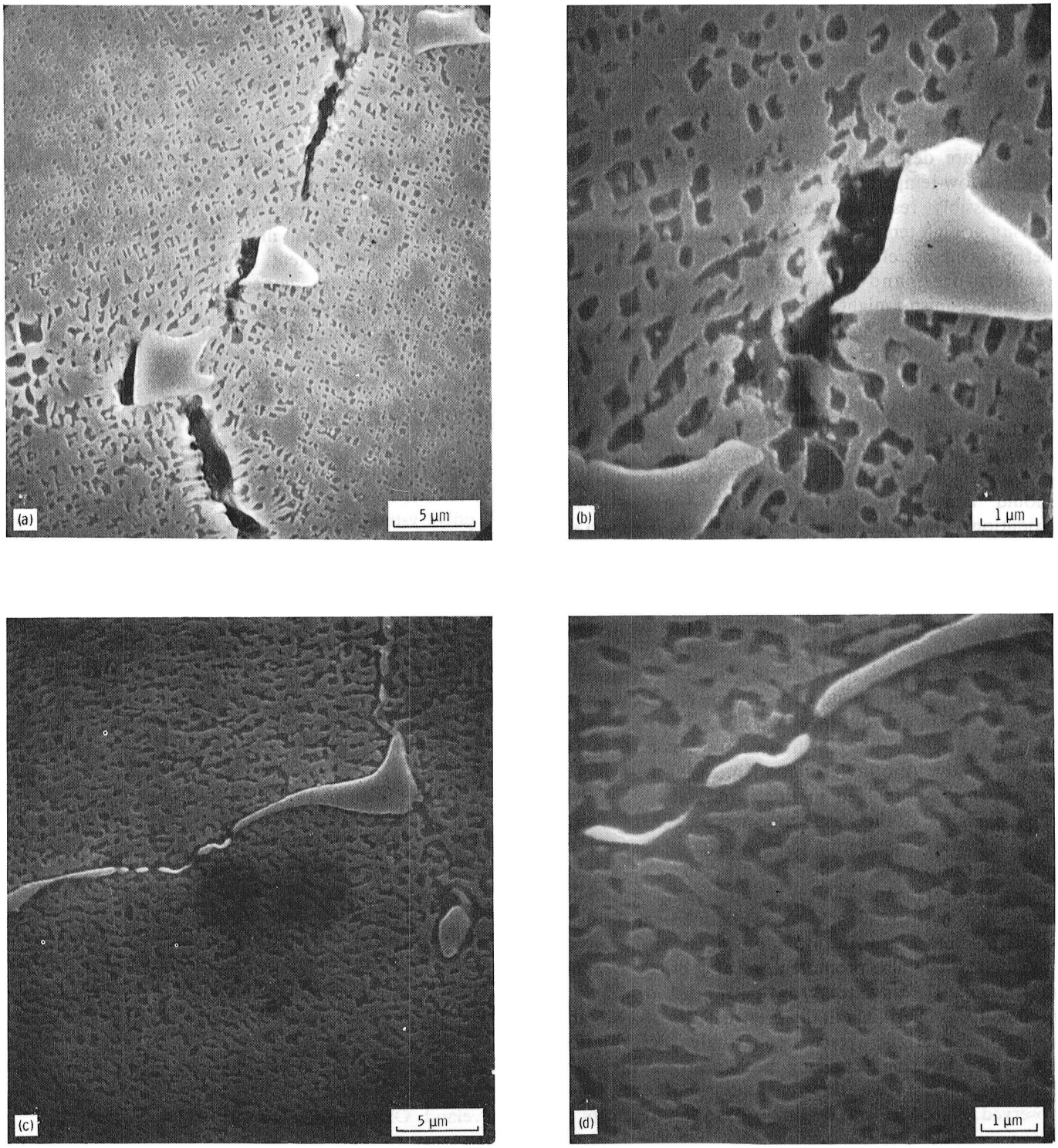

(a) In phase, overview of grain boundary region (specimen HH-66).
(b) In phase, closeup of carbide particle crack.
(c) Out of phase, overview of grain boundary region (specimen HH-53).
(d) Out of phase, closeup of grain boundary region (specimen HH-53).

Figure 11. – Comparison of γ' morphology after in-phase (inelastic strain range $\Delta\epsilon_{in} = 0.0006$, $N_f = 73$) and out-of-phase ($\Delta\epsilon_{in} = 0.0006$; $N_f = 1304$) thermomechanical fatigue cycling to failure of MAR-M 200.

dislocation mechanism, or dislocations must bypass particles by means of a looping mechanism. In effect, the microstructure resulting from high-temperature deformation will include nonglissile dislocations on slip systems that are inactive at low temperatures, dipole loops, twin boundaries, and a generally alien dislocation distribution as compared with that resulting from low-temperature deformation. These features will interact with the low-temperature-deformation micromechanisms and possibly result in increased mobile dislocation density at high temperatures and large numbers of point defects. One net effect of the interaction between high-temperature- and low-temperature-deformation micromechanisms might be rapid void nucleation at grain boundaries, as was in fact observed for Nimonic 80A after it was subjected to low-temperature prestrain followed by high-temperature creep (ref. 18). In-phase cycling would favor more rapid void formation through accelerated diffusion at high temperatures under tensile stresses than under compressive stresses (ref. 19).

Another factor that TMF life prediction methods should address is the environment—in particular, oxidation. Oxidation can contribute to TMF crack growth in a number of ways. For out-of-phase cycling the oxide film grows while the specimen is in compression; during low-temperature tensile deformation this film is likely to crack, leading to a rapid crack initiation process. This mechanism is documented in reference 8 for an austenitic stainless steel. Thus, if this particular mechanism is predominant in nucleating and growing the crack in TMF, the out-of-phase life would be shorter than the in-phase life. Such was not the case in the present study. Another oxidation mechanism, evidence for which was obtained in this investigation, involves rapid oxidation of the plastic zone at the crack tip. This is more apt to operate during in-phase cycling than during out-of-phase cycling because the crack is open at high temperature. This mechanism would also operate under isothermal cycling. Crack tip oxidation can lead to accelerated crack growth through local embrittlement or spalling and can also promote a wedging effect, opening the crack, if outward growth of the oxide film predominates. Certainly in the present series of TMF and isothermal fatigue tests, no single deformation mechanism nor single cracking mechanism was involved. Rather, at least two different modes of each were observed. Since SRP was originally based on a concept of bimodal deformation, the approach might be extended to deal with TMF problems. A clearer micromechanistic understanding will of course be required to pursue such an extension.

The challenges in developing viable TMF life prediction methods lie in identifying the dominant damage mechanisms for a material and set of conditions, and quantitatively modeling these mechanisms from the standpoint of their effect on TMF life. From a data generation point of view, which is largely an economic one, TMF life prediction methods should employ, to the maximum possible extent, isothermal data along with variable-temperature concepts. Considerably more research will be needed to sort out the complexities of this extremely important technological problem.

Conclusions

From the results of this investigation, the following conclusions regarding thermomechanical fatigue (TMF) of polycrystalline MAR-M 200 over the temperature range of 500° to 1000° C were drawn:

1. TMF cycling significantly shortens fatigue life as compared with isothermal cycling at the maximum temperature.
2. Phasing of the TMF cycle has a marked effect on life, with in-phase TMF lives being significantly shorter than out-of-phase TMF lives.
3. In-phase cycling results in extensive internal grain boundary and carbide-matrix interface boundary cracking.
4. Extensive crack tip oxidation occurs after in-phase cycling.
5. Carbide particle fracture results from out-of-phase cycling.
6. None of the isothermal-based life prediction methods considered (spanning factor, strainrange partitioning (SRP), frequency separation, Ostergren's model, and Antolovich's oxidation model) are directly applicable to the TMF results. Most predicted phasing effects were exactly opposite to the observed behavior.

National Aeronautics and Space Administration
Lewis Research Center
Cleveland, Ohio, September 19, 1983

Appendix—Spanning Factor Method

TMF life prediction based on the spanning factor method for cycling between two temperatures, T_1 (minimum temperature) and T_2 (maximum temperature), is given by (ref. 3):

$$N_f(T_1,T_2)=\frac{2[N_f(T_1)/N_f(T_2)]^{1-\delta}}{1+N_f(T_1)/N_f(T_2)}N_f(T_2)$$

where

$$\delta=\frac{2[\beta(T_2)]}{3}$$

Here $\beta(T_2)$ is the slope (absolute value) of the inelastic-strain-versus-life line at T_2 and $N_f(T)$ is the isothermal life at temperature T for a given inelastic strain range. By way of example, consider an inelastic strain range of 0.1 percent in figure 12. Then

$N_f\ (T_1)=132$ where $T_1=500°$ C

$N_f\ (T_2)=2000$ where $T_2=1000°$ C

and δ is 0.51. The TMF life calculated by using the spanning factor is 991 cycles.

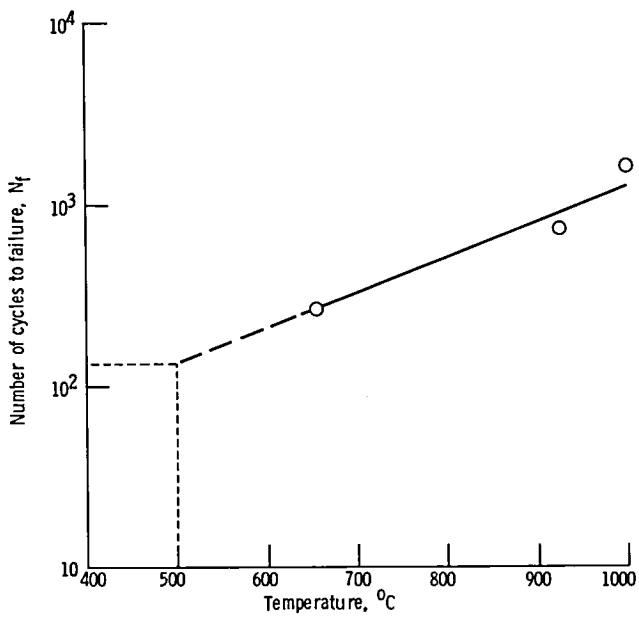

Figure 12.—Cyclic life as function of temperature for polycrystalline MAR-M 200. Inelastic longitudinal strain range, 0.1 percent.

References

1. Bizon, P. T.; Spera, D. A.: Comparative Thermal Fatigue Resistance of Twenty-Six Nickel- and Cobalt-Base Alloys. NASA TN D-8071, 1975.
2. Whittenberger, J. D.; and Bizon, P. T.: Comparative Thermal Fatigue Resistance of Several Oxide Dispersion Strengthened Alloys. Int. J. Fatigue, vol. 3, no. 4, Oct. 1982, pp. 173–180.
3. Taira, S.; Motoaki, F.; and Takashi, H.: A Method for Life Prediction of Thermal Fatigue by Isothermal Fatigue Testing. Proceedings, 1973 Symposium on Mechanical Behavior of Materials, The Society of Materials Science (Kyoto, Japan), 1974, pp. 257–264.
4. Lundberg, L.; and Sandstrom, R.: Application of Low Cycle Fatigue Data to Thermal Fatigue Cracking. Scand. J. Metall., vol. 11, no. 2, 1982, pp. 85–104.
5. Halford, G. R.; and Manson, S. S.: Life Prediction of Thermal-Mechanical Fatigue Using Strainrange Partitioning. Thermal Fatigue of Materials and Components, Am. Soc. Test. Mater. Spec. Tech. Publ. 612, 1977, pp. 239–254.
6. Rau, C. A., Gemma, A. E.; and Leverant, G. R.: Thermal-Mechanical Fatigue Crack Propagation in Nickel- and Cobalt-Base Superalloys Under Various Strain-Temperature Cycles. Fatigue at Elevated Temperatures, Am. Soc. Test. Mater. Spec. Tech. Publ. 520, 1973, pp. 166–178.
7. Hirschberg, M. H.: A Low Cycle Fatigue Testing Facility. Manual on Low Cycle Fatigue Testing, Am. Soc. Test. Mater. Spec. Tech. Publ. 465, 1970, p. 67.
8. Manson, S. S.; Halford, G. R.; and Oldrieve, R. E.: Relation of Cyclic Loading Pattern to Microstructural Fracture in Creep-Fatigue, NASA TM-83473, 1982.
9. Ostergren, W. J.: A Damage Function and Associated Failure Equations for Predicting Hold Time and Frequency Effects in Elevated Temperature Low Cycle Fatigue. J. Test. Eval., vol. 4, no. 5, 1976, pp. 327–339.
10. Coffin, L. F.: The Concept of Frequency Separation in Life Prediction for Time-Dependent Fatigue. 1976 ASME-MPC Symposium on Creep-Fatigue Interaction, R. M. Curran, ed., ASME, 1976, pp. 349–364.
11. Antolovich, S. D.; Liu, S.; and Baur, R.: Low Cycle Fatigue Behavior of René-80 at Elevated Temperature. Metall. Trans. A, vol. 12A, Mar. 1981, pp. 473–481.
12. Characterization of Low Cycle High Temperature Fatigue by the Strainrange Partitioning Method. AGARD-CP-243, 1978.
13. Halford, G. R.; Saltsman, J. R.; and Hirschberg, M. H.: Ductility Normalized-Strainrange Partitioning Life Relations for Creep-Fatigue Life Prediction. Proceedings of the Conference on Environmental Degradation of Engineering Materials, M. R. Louthan and R. P. McNitt, eds., Virginia Tech. Printing Dept., Virginia Polytechnic Institute and State University, 1977, pp. 599–612.
14. McKnight, R. L.; Laflen, J. H.; Halford, G. R.; and Kaufman, A.: Turbine Blade Nonlinear Structural and Life Analysis, J. Aircr., vol. 20, no. 5, May 1983, pp. 475–480.
15. Coply, S. M.; and Kear, B. H.: Temperature and Orientation Dependence of the Flow Stress in Off Stoichiometric $Ni_3Al(\gamma'$ Phase). Trans. Met. Soc. AIME, vol. 239, 1967, pp. 977–984.
16. Hornbogen, E.: High Temperature Materials in Gas Turbines, P. R. Sahm and M. O. Speidel, eds., Elsevier Scientific Publishing Co. (Amsterdam), 1974, p. 195.
17. Dermarker, S.; and Strudel, J. L.: High Temperature Deformation Modes in Nickel Base Superalloys. Strength of Metals and Alloys, Vol. 1, P. Haasen, ed., Pergamon Press, 1979, p. 705.
18. Dyson, B. E.; and Rogers, M. J.: Prestrain, Cavitation, and Creep Ductility. Metal Science, vol. 8, 1974, pp. 261–266.
19. Diffusion, ASM, 1973.

1. Report No.	2. Government Accession No.	3. Recipient's Catalog No.
NASA TP-2280 AVSCOM TR 83-C-6		

4. Title and Subtitle

Preliminary Study of Thermomechanical Fatigue of Polycrystalline MAR-M 200

5. Report Date

February 1984

6. Performing Organization Code

505-33-22

7. Author(s)

Robert C. Bill, Michael J. Verrilli, Michael A. McGaw, and Gary R. Halford

8. Performing Organization Report No.

E-1795

10. Work Unit No.

9. Performing Organization Name and Address

NASA Lewis Research Center
and
Propulsion Laboratory
USAAVSCOM Research and Technology Laboratories
Cleveland, OH 44135

11. Contract or Grant No.

13. Type of Report and Period Covered

Technical Paper

12. Sponsoring Agency Name and Address

National Aeronautics and Space Administration
Washington, DC 20546
and
U.S. Army Aviation Systems Command
St. Louis, MO 63166

14. Sponsoring Agency Code

15. Supplementary Notes

Robert C. Bill: Propulsion Laboratory, USAAVSCOM Research and Technology Laboratories.
Michael J. Verrilli: Northwestern University, Evanston, Illinois.
Michael A. McGaw and Gary R. Halford: Lewis Research Center.

16. Abstract

Thermomechanical fatigue (TMF) experiments were conducted on polycrystalline MAR-M 200 over a cyclic temperature range of 500° to 1000° C. Inelastic strain ranges of 0.03 to 0.2 percent were imposed on the specimens. TMF lives were found to be significantly shorter than isothermal low-cycle-fatigue (LCF) life at the maximum cycle temperature, and in-phase cycling was more damaging than out-of-phase cycling. Extensive crack tip oxidation appeared to play a role in promoting the severity of in-phase cycling. Carbide particle - matrix interface cracking was also observed after in-phase TMF cycling. The applicability of various life prediction models to the TMF results obtained was assessed. It was concluded that current life prediction models based on isothermal data as input must be modified to be applicable to the TMF results.

17. Key Words (Suggested by Author(s))		18. Distribution Statement
Fatigue	Superalloy	Unclassified - unlimited
High temperature	Polycrystalline	STAR Category 26
Thermomechanical	Oxidation	

19. Security Classif. (of this report)	20. Security Classif. (of this page)	21. No. of pages	22. Price*
Unclassified	Unclassified	16	A02

*For sale by the National Technical Information Service, Springfield, Virginia 22161

NASA-Langley, 1984

National Aeronautics and
Space Administration

Washington, D.C.
20546

Official Business
Penalty for Private Use, $300

THIRD-CLASS BULK RATE

Postage and Fees Paid
National Aeronautics and
Space Administration
NASA-451

NASA

POSTMASTER: If Undeliverable (Section 158 Postal Manual) Do Not Return